Creep behavior of C-S-H under different drying relative humidities: Interpretation of microindentation tests and sorption measurements by multi-scale analysis

Piyapong Suwanmaneechot[1], Aili Abudushalamu[1], Ippei Maruyama[1,2,*]

1: Graduate School of Environmental Studies, Nagoya University, Nagoya, Japan

2: Graduate School of Engineering, The University of Tokyo, Tokyo, Japan

i.maruyama@nagoya-u.jp

*: Corresponding author

Abstract

The mechanism behind the creep of concrete is primarily governed by calcium silicate hydrate (C-S-H). The results presented in this study demonstrate the effect of varying relative humidity, water-to-cement ratios, and cement type on the creep properties of hardened cement paste as determined by microindentation. Water vapor sorption and XRD/Rietveld analysis were used to characterize the tested cement paste samples. Multi-scale analysis was also applied to downscale the creep properties of the cement paste to that of the C-S-H gel. When the drying relative humidity decreased, the specific surface area decreased whereas the bulk modulus of the C-S-H gel increased. This increase of creep modulus may be explained by the sliding of C-S-H sheets as lubricated by water molecules. Drying reduces the specific surface area, resulting in increased difficulty in the sliding of C-S-H sheets; hence, the creep modulus increases.

Keywords: Creep (C), Calcium-Silicate-Hydrate (C-S-H) (B), Drying (A), Microindentation (B), Surface area (B)

1. Introduction

Creep, a critical issue in the field of study of cement that has been studied extensively by many researchers with varying perspectives, is the time-dependent deformation of a structure under sustained load throughout its

service life. Creep deformation affects large concrete infrastructure, such as nuclear or hydro power plants and bridges that must withstand extreme environments with large extremes in both humidity and temperature. However, the mechanism behind creep is still not completely understood. Concrete creep primarily results from cement paste, which cannot remain dimensionally stable as compared to aggregate. Additionally, at the micro-scale of the cement paste, the presence of calcium-silicate-hydrate (C-S-H) primarily contributes to concrete creep, as compared to unhydrated clinker and crystalline phases from hydration products [1-5]. C-S-H is the main amorphous phase and is dependent on various factors: mixture, moisture, temperature, curing condition.

Basic creep (i.e. time-dependent deformation without moisture exchange between the concrete and the atmosphere) of concrete/cement paste evolves a logarithmic function of time at long term, as shown by macroscopic tests in [6], nano-indentation tests in [5, 7, 8], and microindentation tests in [9-11]. For the indentation of the cement paste, the time scale for the creep experiments is shortened from a year or month to a minute [11, 12]. This is especially useful for the rapid assessment of long-term creep behavior (i.e. behavior defined by kinetics) for determining the stability and durability performance of concrete structures. Reduced difficulties in macroscopic creep testing are observed, in terms of both the experimental method and environmental sensitivity of the test sample. Alternatively, one of the limitations of the nanoindentation technique is that this method detects the local creep property of C-S-H, and then statistically classifies it as either low density (LD) C-S-H, or high density (HD) C-S-H [13], which do not reflect the creep behavior of the entire C-S-H gel structure. The C-S-H structure, which is affected by sensitivity factors, should consider solid C-S-H, interlayer pores, and small gel pores. In this manner, microindentation can be performed on a large amount of cement paste to cover the entire C-S-H gel structure [10]. To determine creep properties of pure C-S-H gel, the microindentation experiment needs to eliminate the effect of capillary pores, including unreacted clinkers and crystalline phases in the cement paste. These phases have been confirmed to restrain the deformation of cement paste [14-16]. The multiscale models [13, 17] proposed for the primary concrete microstructure levels upscale the mechanical properties obtained by nanoindentation to the scale of the concrete. Later, Aili et al. [18] developed a contrary model that estimates the long-term creep properties of the C-S-H gel using the basic creep data of the concrete.

C-S-H demonstrates colloidal features [19-22], which are influenced by both the chemically bounded water in the C-S-H and evaporable water. Our previous publications [23-26] found that the C-S-H microstructure evolves with change in moisture. C-S-H agglomerations during the long-term drying process, resulting from water that is removed, are attributed to the arrangement of C-S-H sheets, as explained by the stacking process (from small-angle x-ray scattering) and decrease of basal spacing of the C-S-H (from water vapor sorption) [26]. This basal spacing is found to decrease when relative humidity decreases from a saturated condition to 40% and remains stable below 40% relative humidity (from short-term length change isotherms and water vapor sorption) [23]. Recently, results from ^{1}H NMR relaxometry investigating water molecule exchange in different pore sizes showed the existence of moveable C-S-H sheets [25]. As for creep, water has a significant impact on large- and small-scale creep behavior [9, 27-32]. Under sealed conditions, wet specimens trend to creep more than dried specimens. Several theories of creep related to water have been proposed, e.g. the sliding of each other gel particles that are lubricated by water [28], the microprestress-solidfication theory of the disjoining pressure of the adsorbed water in micropores [33], the dissolution-precipitation mechanism in a moist condition [31], and the microcracking theory, which considers holding loads including effect of water movements inducing basic creep [34, 35]. However, the creep mechanism of C-S-H gel and the role of water have not been yet fully understood.

The aim of this study is to experimentally investigate the creep of hardened cement paste (hcp) that is dried under different relative humidity conditions for a long time. The microindentation technique is applied to measure the creep properties of cement paste. An experimental campaign was conducted under a full range of relative humidity (from 100% to 11% relative humidity) for the drying, which is a wider range than those presented in literature [9]. The phase composition of the cement pastes are evaluated using a XRD/Rietveld analysis, while porosity is obtained from water vapor sorption measurements. Then, combining the phase composition and porosity with a multi-scale model, creep properties are downscaled from the cement paste to the C-S-H gel. Creep of C-S-H gel is explained by agglomeration of C-S-H and by sliding of C-S-H sheets. Finally, we compare our results with two models from literature: the microscopic relaxation model proposed by Vandamme [36] and the atomistic simulation of Morshedifard et al. [37].

2. Experimental programs

2.1 Cement properties

Two types of cement were considered in this study. The chemical components and mineral compositions of low heat Portland cement (L) and high early strength Portland cement (H) are shown in Table 1 and Table 2. The proportion of the main phases in cement clinker was evaluated by Rietveld x-ray diffraction quantification.

Table 1

Chemical composition of the low heat (L) and high early strength Portland cement (H) as found by x-ray fluorescence analysis (mass %).

Cement	SiO_2	Al_2O_3	Fe_2O_3	CaO	MgO	K_2O	Na_2O	SO_3	LOI	Na_2O eq	Cl-	Total
H	20.46	4.96	2.49	65.71	1.48	0.33	0.20	2.90	0.78	-	0.014	99.324
L	25.85	3.32	3.08	62.28	0.76	0.25	0.19	2.84	0.73	0.35	0.003	99.653

Table 2

Mineral composition of Cement H and L as determined by Rietveld x-ray diffraction quantification (mass %).

Cement	C_3S	C_2S	C_3A	C_4AF	Periclase	Bassanite	Gypsum	Total
H	65.56±2.20	15.14±0.93	6.75±0.29	7.96±0.47	0.81±0.28	2.39±0.20	0.51±0.66	99.12
L	20.11±1.60	62.95±1.14	1.95±0.43	10.71±0.60	0.52±0.22	2.43±0.36	1.11±0.63	99.78

C: CaO, S: SiO_2, A: Al_2O_3, F: Fe_2O_3

2.2 Specimen preparation

The cement pastes were made from low heat Portland cement and high early strength Portland cement with a water-to-cement ratio of 0.30 and 0.55. The Portland cement was mixed with water in a paddle mixer at room temperature. After that, the fresh paste was moved to a thermostatic room at 20 ± 1 °C and was remixed by hand every 30 minutes for 6 hours to reduce the effect of bleeding. In this study, 3 × 13 × 100 mm specimens were cast and sealed. Demolding was done three days after casting, then cured in lime-saturated water for 1 year and the

specimens were placed into chambers with controlled humidity for three years The thickness of bar specimen (3 mm) was selected to prevent contraction-induced microcracking on the surface due to gradient of moisture content [38]. Prior to the test, samples were observed by microscope and no crack was found.

For drying, the low heat Portland cement paste was stored in a chamber in which the relative humidity was controlled by a saturated salt solution as shown in Table 3 [39]. The high early strength Portland cement paste was dried in chambers whose relative humidity was controlled by sodium hydroxide solutions with varying concentrations as shown in Table 4 [40]. 10 specimens were placed directly on a metal mesh with sieve opening of 8 mm over chemical solution of ~100 ml for controlling relative humidity in the chamber (35 × 130 × 185 mm). In case of L cement paste, saturated solutions were used to control relative humidity. Since more salt surpassing the solubility were added in preparation of saturated solution, even with release of water from sample, solution remained still saturated. Hence, relative humidity did not change. In case of H cement, sodium hydroxide solution with different concentration were used to control relative humidity. Based on the drying protocol established [24], sodium hydroxide solution were replaced every two weeks in the beginning to keep the relative humidity at expected value, until no significant increase (less than 2%) of relative humidity measured. By doing so, severe drying and carbonation were also avoided. Drying lasted for more than three years for the two cements. The lengthy drying time was selected to achieve not only a relative humidity equilibrium but also to let the microstructural changes of C-S-H fully complete [24]. The dried cement paste at a target relative humidity is denoted as LXX_YYRH or HXX_YYRH, where XX is the water-to-cement ratio and YY is the relative humidity. Furthermore, LXX_100RH and HXX_100RH were immersed in lime-saturated water just after demolding until testing.

Table 3

Saturated salt solution for controlling relative humidity.

RH (%)	11	33	40	58	79	85	95
Saturated salt	$LiCl_2$	$MgCl_2$	NaI	NaBr	NH_4Cl	KCl	KNO_3

Table 4

Concentration of sodium hydroxide in the aqueous solution.

RH (%)	11	20	30	40	50	60	70	80	90	95
Concentration (%mass)	47.97	40.00	35.29	31.58	28.15	24.66	20.80	16.10	9.83	5.54

2.3 Characterization of the cement paste during drying

2.3.1 XRD/Rietveld analysis

After drying in their respective chambers for three years, the specimens were tested by the x-ray diffraction method (D8 ADVANCE, Bruker AXS). The specimen hydration was arrested by isopropanol and kept in the 11% relative humidity desiccator at 20 °C for two weeks to eliminate the isopropanol. Then, the specimens were ground after hydration ceased, with the 10% Corundum powder (α-Al_2O_3 by mass) used as a standard reference for quantifying the phase compositions. The tube voltage, tube current, scan range, step width, and scan speed for the XRD was 40 kV, 40 mA, 2θ, 2-65°, 0.02°, and 0.5°/min, respectively. Phase compositions of the cement paste were calculated from the Rietveld analysis (TOPAS 4.2, Bruker AXS) based on [41]. Three identical samples were tested for each set of drying states. The mass ratio of reacted clinker over initial clinker was defined as hydration degree.

2.3.2 Sorption measurements

The water vapor sorption isotherms were measured at 20 °C by the volumetric method using the VSTAR (Quantachrome instrument) for investigating mesopores and micropores under different relative humidities. The samples were ground until particles passed through a 75 μm sieve and retained on a 25 μm sieve. The initial state of sample in our instrument should be under vacuum condition. Hence, as pretreatment method, a 25 ± 1 mg sample in terms of wet mass was dried by a vacuum pump to obtain the fully dry specimen at 20 °C prior to measurement. In every measurement, starting from vacuum condition, the water molecules are introduced into the cell step by step to control the relative pressure. On adsorption branch, the relative pressure started from 0, increased until the peak; then decreased to ~0.005 on the desorption branch. At each step of measurement, if change of pressure in the cell is less than 0.1 Torr (i.e., 13.3 Pa) during 2 minutes, it was supposed that the equilibrium was reached and system moved to the next measurement point. Otherwise, measurement continued

144 in this step by introducing more water vapor into the cell or removing water vapor from the cell. The sorption
145 isotherm was built step by step by estimating the incremental water vapor for incremental increasing pressure at
146 equilibrium. At the end of the measurement, the sample was again vacuum dried in a heating mantle at 105 °C to
147 obtain the dry mass for normalizing the sorption amount. The Brunauer-Emmett-Teller (BET) theory [42] was
148 applied on the adsorption branch (relative pressure between 0.05 and 0.35) to calculate the specific surface area
149 (S_{H2O}) by taking the cross section of one water molecule equal to 0.114 nm² [43].
150 Additionally, for each drying relative humidity, a dried sample block was taken out and its initial mass W_0 was
151 measured. Then, this sample block was re-saturated in lime-saturated water under vacuum for 24 hours at room
152 temperature and the saturated mass W_{sat} was then measured. Finally, the samples were dried in an oven at 105 °C
153 for two weeks and the dried mass W_{dry} was measured. The water capacity was then calculated as $(W_{sat} -$
154 $W_{dry})/W_{dry}$. The oven-dry mass at 105 °C was chosen to be reference as it is supposed that only evaporable water
155 is removed from hcp at 105 °C similar to [24, 44, 45].
156
157 2.4 Creep analysis by microindentation
158 The creep properties were examined by the microindentation technique. A small bar specimen piece was
159 embedded in epoxy resin in a cylindrical mold (25 mm diameter, 22 mm height). After the epoxy resin was
160 sufficiently cured, the samples were cut into 5 mm thicknesses by a high-precision diamond band saw (EXAKT
161 300). Then, the specimens were stored in the original chamber for at least two weeks to recover the relative
162 humidity equilibrium prior to measurement.
163 Microindentation tests were performed under load control with the Shimadzu Autograph AGS-X. A
164 trapezoidal loading history was used for the creep assessment, with a maximum load of P_{max} = 20 N. The load was
165 applied at a rate of 1.333 N/s, then kept steady over 300 s and unloaded at the same rate as initially applied, as
166 shown in Fig. 1. This loading and unloading rate were selected for following the typical value in literature [9, 11].
167 For this study, a Berkovich indenter was used, which has a triangular-based pyramid and a 62.12° semi-apex angle
168 of the indenter. The indentation tip response was recorded by a laser displacement meter (Keyence LK-G30) with
169 an accuracy of 0.01 μm. During testing, the specimens were enclosed in a hermetic chamber to avoid carbonation

and to maintain the relative humidity at 20 ± 1 °C by using the chemicals as shown in Table 3 and Table 4. Moreover, a moving table with a stepping motor controller was used to make equidistance indentations (0.75 mm). The indentation test was performed on more than fifteen points for each set of drying states for each sample.

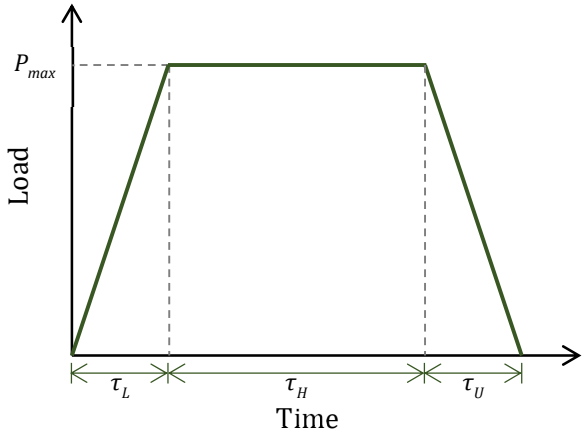

Fig. 1. A typical load history of the microindentation tests.

After withdrawing the indenter from the indented surface, the diameter of the indent has a minor change. The projected residual indent area on the surface of the tested material is comparable with the maximum contact area A_c during the indentation test. The maximum depth consists of two parts: a depth h_c at which the indenter touches the indented surface and a depth $h_s$at which the indenter does not touch the indented surface:

$$h_{max} = h_c + h_s \tag{1}$$

Knowing the depth h_s for a conical indenter [46], Eq (1) yields

$$h_c = h_{max} - \varepsilon \frac{P_{max}}{S} \tag{2}$$

where S is an initial slope of the unloading branch, and the geometric constant ε is equal to 0.72 for a conical indenter. Therefore, the contact area is [9]

$$A_c = 3\sqrt{3}h_c^2 \tan^2\theta \tag{3}$$

Based on the same indented surface, the contact radius a_c can be defined as

$$a_c = \frac{\sqrt{A_c}}{\sqrt{\pi}} \quad (4)$$

Four properties were evaluated: the creep coefficient and contact creep modulus from the holding phase, and the indentation modulus and hardness from the unloading phase. The ratio between the maximum depth and the initial depth during the holding period is defined as the creep coefficient C.

$$C = \frac{h_{max} - h_{ini}}{h_{ini}} \quad (5)$$

The depth gradually increases with time when the load is kept constant. The contact creep function $L(t) - L(0)$, which describes the time-independent behavior, is given as [11]

$$L(t) - L(0) = \frac{2a_c \Delta h(t)}{P_{max}} \quad (6)$$

where $\Delta h(t)$ is the change of the indentation depth during the holding period. Since the long-term creep behavior is observed to vary as a logarithmic function of time [9, 11] , the measured indentation creep data can be given by

$$L(t) - L(0) = \frac{\ln (t/\tau_i + 1)}{C^M} \quad (7)$$

The parameter $C^M$and τ_i are the contact creep modulus and characteristic time, respectively.

Since microindentation induces locally very high-stress, force/deformation relation is nonlinear at the beginning. Elastic properties, i.e., indentation modulus and indentation hardness, should be considered on the unloading branch. The indentation modulus M was found from the initial slope S of the unloading branch of the load-displacement curve, while the indentation hardness H was calculated as the mean pressure applied on the sample at the maximum load. Both parameters are defined by

$$M = \frac{S\sqrt{\pi}}{2\beta\sqrt{A_c}} = \frac{S}{2\beta a_c} \quad (8)$$

and

$$H = \frac{P_{max}}{A_C} \quad (9)$$

3. Results

3.1 XRD/Rietveld analysis

Fig. 2 shows the degree of hydration of the cement clinker (summation of all clinker minerals) in H-hcp and L-hcp under different relative humidities. The drying condition was found to not significantly affect the degree of hydration, implying that hydration almost fully completed during the one-year-cure cycle under lime-saturated water before drying. H55 had the highest degree of hydration, followed by L55, H30, and then L30. The degree of hydration approached more than 90% for a w/c ratio of 0.55 and more than 75% for w/c ratio of 0.30. Under different relative humidities, the degree of hydration of the cement clinker decreased slightly from 80% to 40% relative humidity, while the degrees of hydration seem to be independent for the other relative humidities. These results were also similar to the results for white hcp as reported by Maruyama et al. [24].

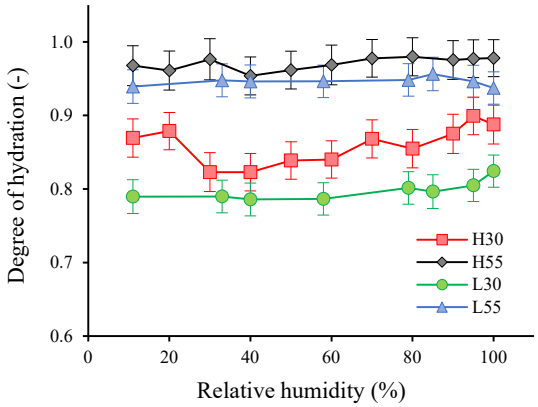

Fig. 2. Degree of hydration of the cement clinker in hcp after drying for three years.

The unreacted clinkers and hydration products from the Rietveld analysis were identified. The phase compositions were obtained through an iterative calculation process [41]. The volume fraction results were normalized per 1 cm^3 of hcp at the sealed condition, as displayed in Fig. 3. The amorphous phases (i.e. C-S-H, C-A-H, and C-F-H) and portlandite (denoted as CH) remained relatively constant for each drying relative humidity for both L-hcp and H-hcp, as the samples were almost fully hydrated before drying. The amount of portlandite in the H-hcp was approximately twice that of L-hcp because the alite phase generated more portlandite than belite phase.

The portlandite was not affected by drying. In the case of ettringite (denoted as Ett), it decomposed at lower relative humidity, however it could not decompose under strong drying conditions [47]. The other crystalline phases - e.g., monosulfoaluminate (denoted as Ms), monocarbonate (denoted as Mc), hemicarboaluminate (denoted as Hc), and hydrogarnet (denoted as Hg) - were present in minor quantities (less than 4%). Moreover, amount of water in hardened cement paste was denoted as H in Fig. 3.

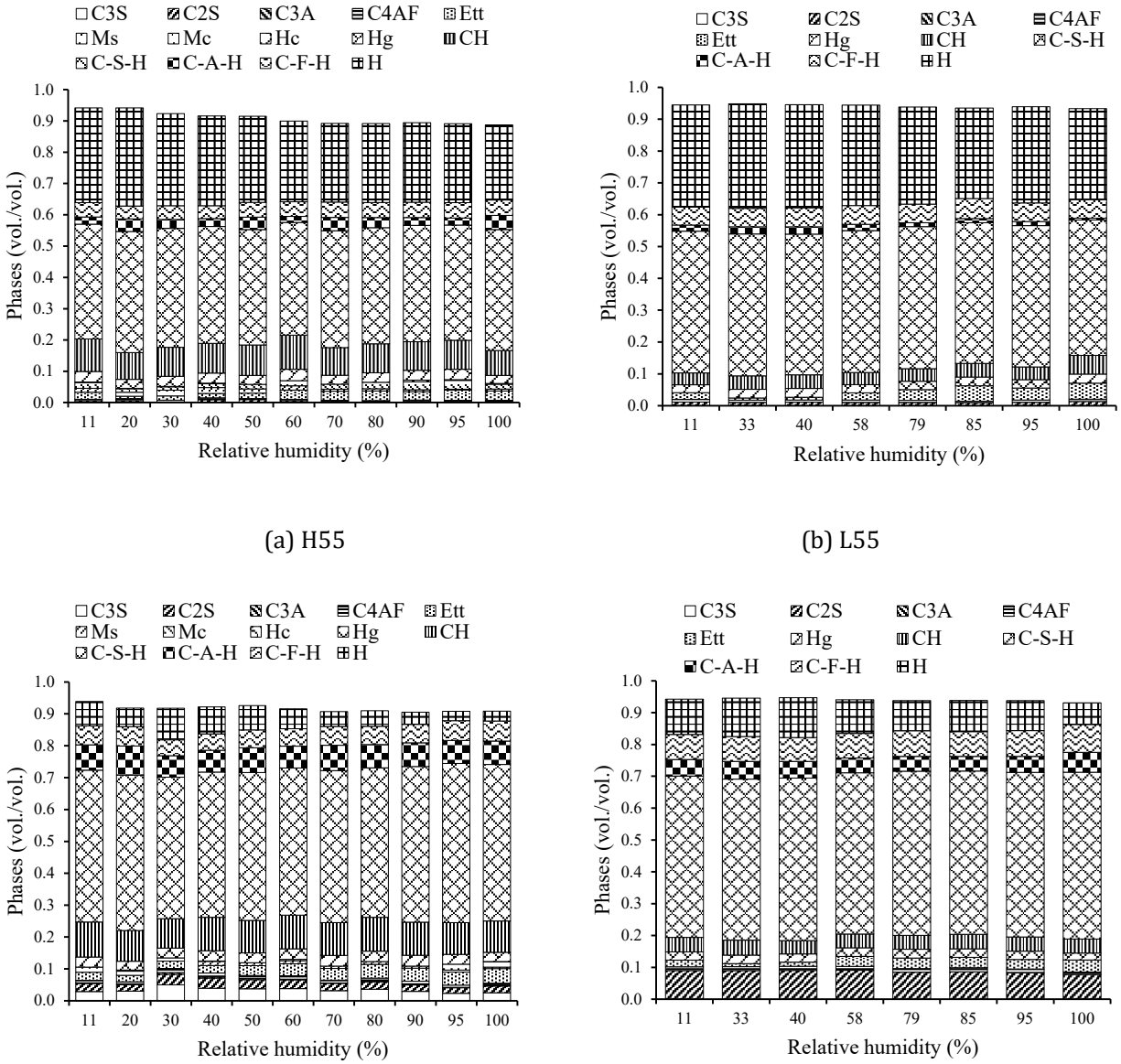

(a) H55 (b) L55

(c) H30 (d) L30

Fig. 3. Phase diagram of the hcp under the sealed condition.

3.2 Water vapor sorption

Before re-saturating the samples, the dried block sample weights W_0 were measured to obtain the water content in the hcp dried under different relative humidity. The water content in the hcp can be seen as the evaporable water content as shown in Fig. 4. In general, the amount of evaporable water decreased dramatically from the saturated condition to 40% relative humidity and there was no significant change from 40% to 11% relative humidity. Fig. 5 shows the re-saturated water content of both hcp samples at various relative humidity. For L55 and H55, for lower relative humidity, the saturated water content is reduced. For L30 and H30, the drying condition did not affect the re-saturated water content.

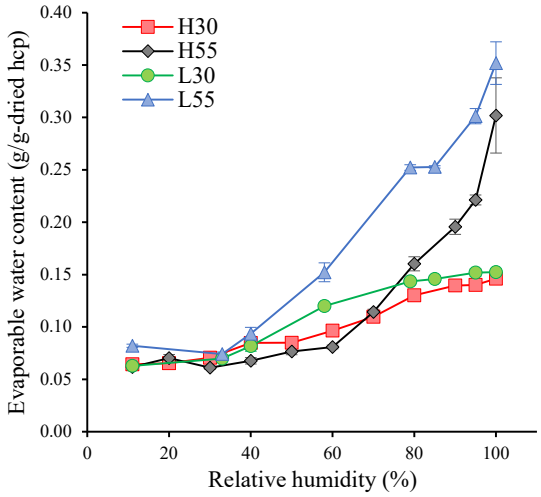

Fig. 4. Evaporable water content of the dried samples at different relative humidities.

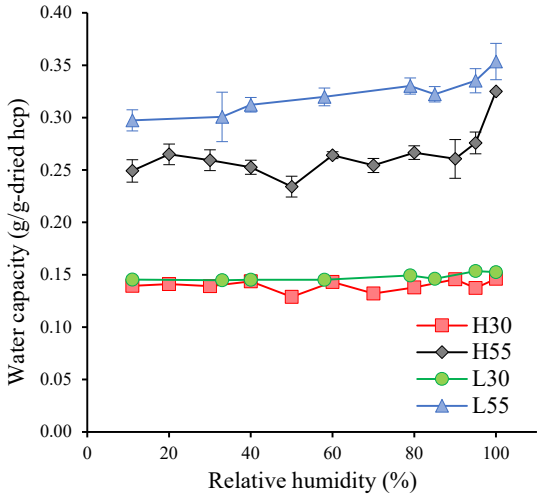

Fig. 5. Saturated water content of the re-saturated samples at different relative humidities.

The water vapor sorption isotherms of the H55 and L55 samples dried under different relative humidities are presented in Fig. 6. The y-axis of Fig. 6 was shifted to better show the shape of isotherm. The shape of the sorption isotherms of higher relative humidity samples (from H55_100RH to H55_60RH and L55_100RH to L55_58RH) were consistent, with a sudden drop (relative pressure between 0.30 and 0.35) observed on the desorption branch. This sudden drop is not clearly#evident on samples with 40% to 50%, where the hysteresis loops are a narrow curve. However, the sudden drop is recovered on lower relative humidity samples (from 30% to 11% relative humidity). Furthermore, in the case of H55, the sorption curve at higher relative pressure (above 0.80) for the lower relative humidity samples was quite precipitous. As for L55, this kind of precipitous increase of adsorption branch at high relative pressure were observed for both low relative humidity sample and also for high relative humidity sample. Moreover, the amount of total sorption still decreased from the saturated condition to 50% relative humidity, and then increased from 50% to 11% relative humidity. Similar trends are observed for the H30 and L30 hcp samples. Note that, hysteresis loop was observed between adsorption and sorption branch of isotherms. The hysteresis for the relative pressure higher than 0.35 (where sudden drip of desorption branch can be observed due to cavitation) is attributed to ink-bottle effect [48, 49]. As for the hysteresis at relative pressure lower than 0.35, is needed more time for pulling out the adsorbed water in very small slit pores (i.e. interlayer spaces in C-S-H). The suction of adsorbed water below relative pressure of 0.35 in VSTAR was limited by time and

lowest relative pressure, so the ending point on desorption branch cannot recover to the beginning point of the adsorption branch. In addition, the different shape of sorption isotherm depended on the initial relative humidity of hcp, reflecting the microstructural change of C-S-H due to the lengthy drying time [23, 24, 26].

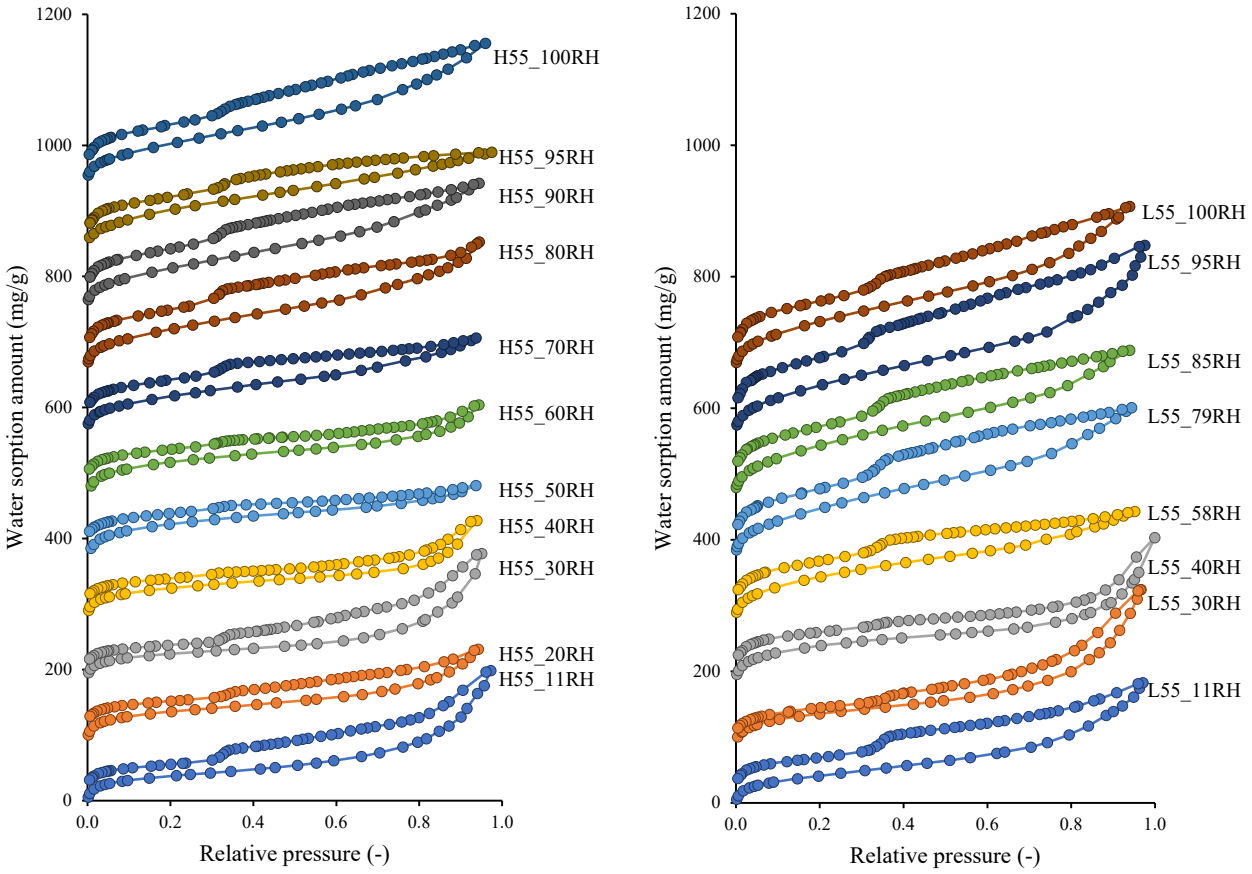

(a) H55 hcp (b) L55 hcp

Fig. 6. The water vapor sorption isotherms for H55 and L55 hcp samples dried at different relative humidities.

The adsorption branches of hcp dried at different relative humidities are shown in Fig. 7. For the samples dried above 79% relative humidity, no differences can be observed on the adsorption branches for relative pressures between 0 and 0.40. As for elevated relative pressures (i.e., 0.40-0.98), the samples dried at lower relative humidity showed lower sorption amounts. For samples dried below 79% relative humidity, the amount of adsorption clearly decreased with decreasing drying relative humidity, this being due to changes in the hcp

microstructures. The pores in the hcp can be classified based on the water vapor sorption. dW_{40-0} is defined as the incremental sorption from the dry condition at 105 °C to relative pressure 0.40 and is associated with the micropores including interlayer spaces [19, 24]. Then, dW_{75-40} is defined as the adsorption capacity from a relative pressure of 0.40 to 0.75 and is related to the mesopores (i.e. gel pores). The change of slope on the adsorption branch at a relative pressure of 0.75 (see Fig. 7) is considered as the fine end of the capillary pores. Combining the water capacity of the re-saturated samples with the water sorption isotherms, the incremental water sorption from a relative pressure of 0.75 to the re-saturated state (dW_{100-75}) was calculated to reflect the macropores in the hcp (i.e. capillary pores). The water sorption proportions of the samples dried at various relative humidities are shown in Fig. 8. For higher w/c ratio, the dW_{100-75} decreased from 100% to 90% relative humidity, increased from 90% to 40% relative humidity and then decreased slightly from 40% to 11% relative humidity. For lower w/c ratio, the samples dried at higher relative humidity have a lower dW_{100-75} than those dried at lower relative humidity. For each cement paste type, the samples dried at lower relative humidity can be observed to have lesser quantities of micropores and mesopores than those dried at higher relative humidity, which can be considered as evidence of agglomeration of the C-S-H due to the release of water from the interlayer space and gel pores. The dW_{40-0} of the L-hcp was slightly greater than that of the H-hcp.

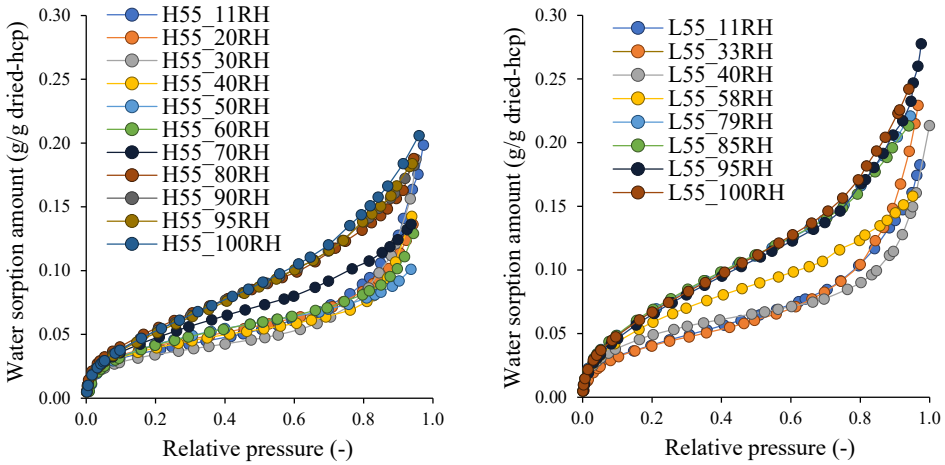

(a) H55 hcp (b) L55 hcp

Fig. 7. The adsorption branches of the H55 and L55 hcp samples dried at different relative humidities.

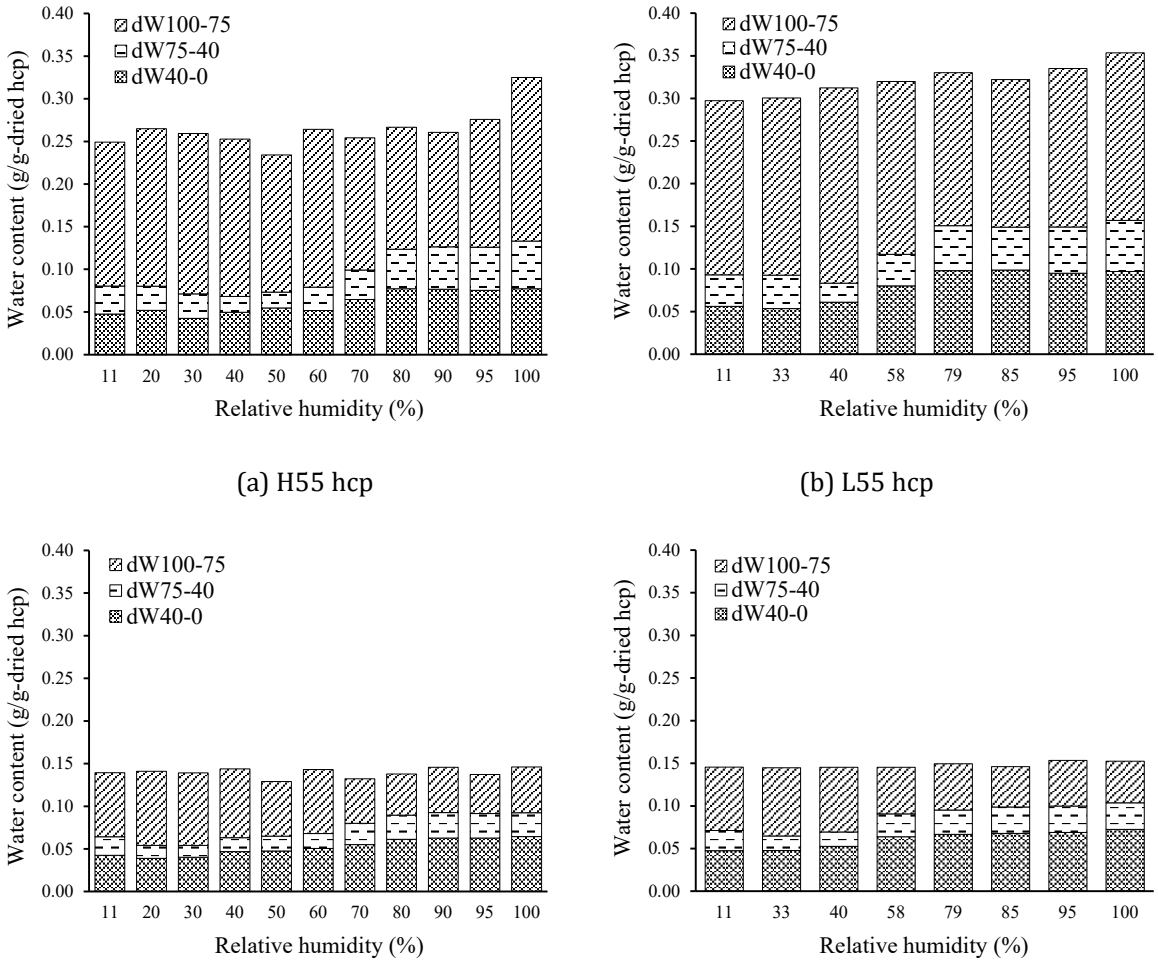

(a) H55 hcp (b) L55 hcp

(c) H30 hcp (d) L30 hcp

Fig. 8. The water sorption proportions of the samples dried at different relative humidities.

The BET surface area was obtained using the adsorption isotherm between the relative pressures of 0.05 and 0.35, following the method presented in [43]. Fig. 9 presents the specific surface area S_{H2O} of the hcp as a function of the drying relative humidity. For one type of hcp, the surface area did not change when the drying relative humidity decreased from 100% to 80%. From 80% to 40% relative humidity, the surface area decreases. When the drying relative humidity is further decreased to 11%, the surface area did not change significantly. H30 and L30 had a lower specific surface area than H55 and L55. S_{H2O} was reduced and remained constant at lower relative humidity. In a prior study, Maruyama et al. [24] demonstrated the sharp decrease in S_{H2O} from 40% to

11% relative humidity. This difference is hypothesized to result from pre-treatment, as contrary to the present study, Maruyama et al. [24] dried the samples at 105 °C, which may have caused decomposition of some hydrates especially at lower drying relative humidity (i.e., RH=11%-30%).

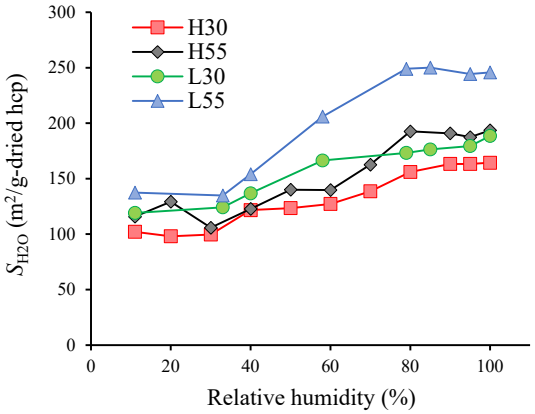

Fig. 9. Specific surface area S_{H2O} of the hcp samples dried at different relative humidities.

3.3 Microindentation

The creep experiments of both cement pastes yielded the contact creep function as shown in Fig. 10. It can be observed that the creep strain magnitude increased with increasing relative humidity. In a consistent manner with the results obtained for different water-to-cement ratios, the creep strain increased with higher water-to-cement ratios [11]. To compare the effect of different drying conditions, the experimental contact creep function was curve fitted with Eq. (7). Fig. 10 further presents the best fits for each relative humidity. The changes in the drying process results in different slopes of the contact creep function [46].

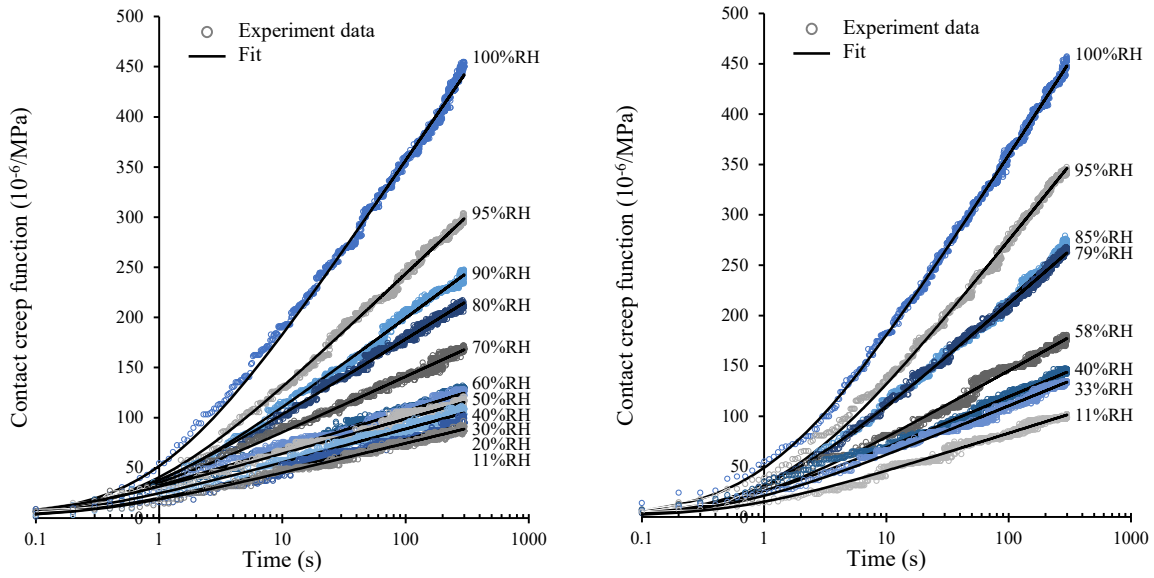

(a) H55 hcp (b) L55 hcp

Fig. 10. Examples of the contact creep functions and best curve fits for the hcp samples dried at different relative humidities.

The creep coefficient of hcp decreases continuously as the relative humidity is decreased (see Fig. 11) which means that the creep strain of hcp at higher relative humidity tends to increase more. This result is verified by the creep coefficients for all four cement pastes presented in Fig. 11. Another observation is that, for the same w/c ratio and the same relative humidities, the coefficient for H-hcp is less than L-hcp. From the lowest drying relative humidity, the curves of both hcp converged at the saturated condition for w/c = 0.55. For one type of cement, above a drying relative humidity of 70% the lower w/c ratio exhibited a lower creep coefficient while below 70% the creep coefficient was higher for a lower w/c ratio. For H30, with further decrease of relative humidity lower than 70%, the initial depth h_{int} (equivalently elastic strain) decreases significantly, resulting in higher creep coefficient comparing to H55. The maximum depth h_{max} for all specimens was between 0.063 and 0.138 mm.

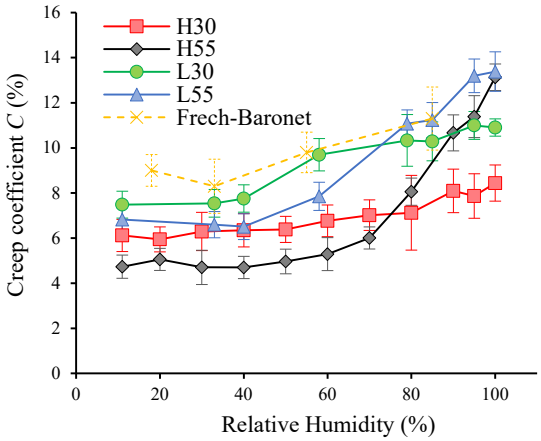

Fig. 11. The creep coefficients of the hcp dried at different relative humidities.

As for creep properties, the contact creep modulus and creep characteristic time are presented as functions of drying relative humidity in Fig. 12 (a) and (b), respectively. The drying condition influences the creep properties as confirmed by the creep modulus and the creep coefficient. For all drying relative humidities, the cement pastes with lower w/c ratios demonstrate higher contact creep moduli. For the same drying relative humidity and the same w/c ratio, H-hcp has a higher contact creep modulus than L-hcp. For all four cement pastes, the contact creep modulus was higher for the lower drying relative humidity. In addition, Frech-Baronet also reported the effect of relative humidity on the creep modulus, with a similar trend observed as presented in Fig. 12 [9]. The decrease of the w/c ratio resulted in an increase in the contact creep modulus.

According to Fig. 10, the experimental contact creep functions demonstrate the logarithmic trend with respect to time, with the starting point of logarithmic kinetics interpreted as the characteristic time. At a high drying relative humidity, the hcp spent more time to reach logarithmic kinetics than at a lower relative humidity. Furthermore, the L-hcp has a higher characteristic time over the range of relative humidities for each w/c ratio as compared with H-hcp. This indicates that the cement type has stronger influence on the characteristic time than the w/c ratio.

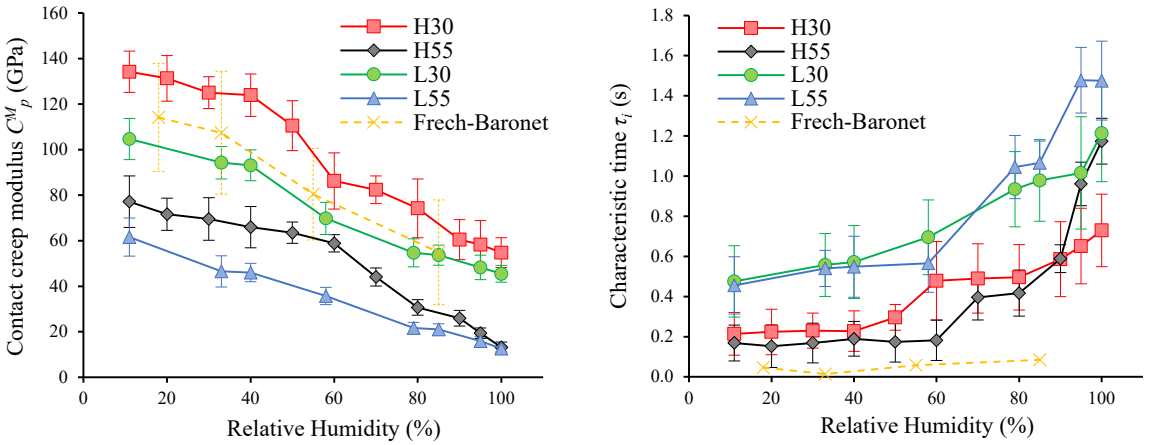

(a) Contact creep modulus (b) Characteristic time

Fig. 12. Fitting parameters obtained from the analysis of the hcp dried at different relative humidities.

The indentation modulus and the indentation hardness of hcp dried at different relative humidities are shown in Fig. 13. Overall, a decrease of the w/c ratio entailed an increase in the indentation modulus [9, 29]. For the same drying condition and w/c ratio, the H-hcp had a higher indentation modulus than the L-hcp. For all four cement pastes, the indentation modulus was higher for lower relative humidity. Between 11% and 100% relative humidity, the indentation modulus was significantly higher for the lower w/c ratio. As expected, the decrease in relative humidity increased the indentation hardness, with similar trends observed to the varying indentation modulus with relative humidity and w/c ratio. In contrast, the L-hcp had a higher indentation hardness than the H-hcp.

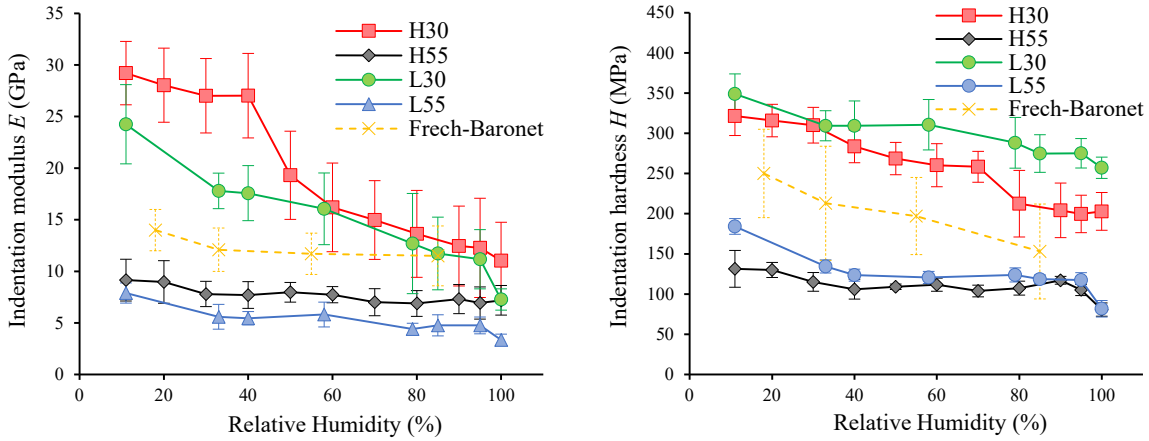

(a) Indentation modulus (b) Indentation hardness

Fig. 13. Mechanical properties obtained from indentation testing as a function of relative humidities.

The fitted parameters of the indentation experiments (i.e., indentation modulus, indentation hardness, creep coefficient, contact creep modulus, characteristic time, and maximum depth) are listed in エラー! 参照元が見つかりません。 to エラー! 参照元が見つかりません。 with the standard deviation in the supplementary data.

4. Long-term creep mechanism of C-S-H gel

Creep of cementitious materials can be commonly categorized by kinetics, referring to different time scales, as short-term creep and long-term creep [50]. In a macroscopic creep experiment, short-term creep takes a few days, while the testing period for long-term creep varies from months to years. Microindentation experimentation on cement paste provides the logarithmic creep compliance for long-term creep as shown in Fig. 10, which is comparable to that obtained from macroscopic creep experiments yet obtained much quicker [11, 13]. It is widely accepted that creep of concrete originates from C-S-H gel (including micropores and mesopores) [5]. Since creep properties from microindentation are also influenced by other cement paste phases, multi-scale analysis is applied in the following sections in order to obtain the creep properties of C-S-H gel. Finally, the creep mechanism of C-S-H gel will be discussed.

398

399 4.1 Creep modulus of C-S-H gel by downscaling

400 Aili et al. [18] developed a#model to estimate the long-term creep properties of C-S-H gel from the creep
401 properties of concrete. This model was applied in this study by considering hcp as a multiscale composite material
402 (as shown in Fig. 14). At the scale of cement paste (see Fig. 14 (a)), crystalline phases from hydration products
403 (e.g., portlandite, ettringite, monosulfoaluminate) and unreacted clinkers are assumed as spherical inclusions,
404 which do not creep, and are embedded in a matrix which is the mixture of C-S-H gel with capillary pores (i.e.
405 macropores). This mixture is supposed to creep. At a lower scale, this mixture of C-S-H gel with capillary pores is
406 supposed to be composed of a matrix of C-S-H gel which embeds capillary pores as shown in Fig. 14 (b). The
407 contact creep modulus C^M determined experimentally is related to the bulk creep modulus C^K through [13, 18]

$$C^M = \frac{3(1-2\nu)}{1-\nu^2} C^K \qquad (10)$$

408

409 Moreover, Aili et al. [51] showed by analyzing experimental results from literature that the long-term
410 viscoelastic Poisson ratio of hcp and of a mixture of C-S-H gel with capillary pores could be assumed to be equal
411 to 0.2.

412 The downscaling from the bulk creep modulus C_p^K of hcp to the bulk creep modulus C_{gel}^K of C-S-H gel is given
413 by [18]

$$C_{gel}^K = \left(\frac{1-f_b}{1+f_b}\right)\left(\frac{1+\phi_c}{1-\phi_c}\right) C_p^K \qquad (11)$$

414

415 where f_b is the volume fraction of unreacted clinkers, portlandite, ettringite, monosulfoaluminate,
416 monocarbonate, hemicarboaluminate, and hydrogarnet with respect to the volume of hcp at the sealed condition.
417 ϕ_c is the volume fraction of the capillary pores with respect to the volume of the mixture of C-S-H gel with capillary
418 pores. The volume fraction f_b of crystal hydrates and unreacted clinker with respect to the volume of cement paste
419 at scale (a) of Fig. 14 is found as

$$f_b = f_{\text{clinker}} + f_{\text{crystal}} \qquad (12)$$

420

421

where f_{clinker} is the sum of the volume fractions of unreacted clinkers (i.e. alite, belite, aluminate, and ferrite) (see エラー! 参照元が見つかりません。 to エラー! 参照元が見つかりません。 in the supplementary data) , and f_{crystal} is the sum of volume fractions of portlandite, ettringite, monosulfoaluminate, monocarbonate, hemicarboaluminate, and hydrogarnet (see エラー! 参照元が見つかりません。 to エラー! 参照元が見つかりません。 in the supplementary data). In those tables, standard deviation contains analytical error from Rietveld analysis and repeatability error (three identical samples).

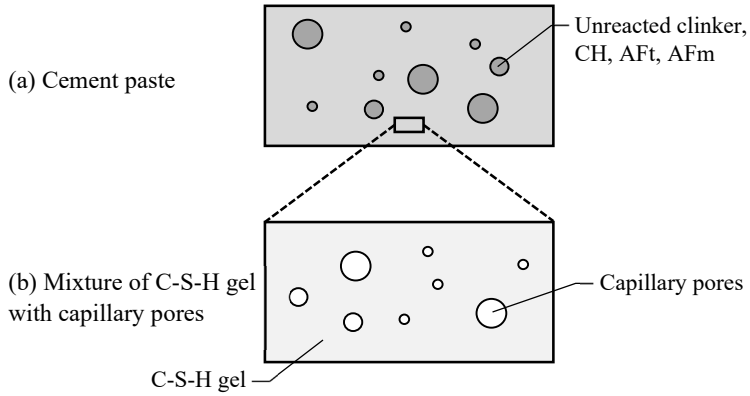

Fig. 14. Multiscale structure of cement paste.

The volume fraction of capillary pores with respect to the mixture of C-S-H gel with capillary pores (see scale (b) in Fig. 14) is

$$\phi_c = \frac{f_{\text{cp}}}{1 - f_{\text{clinker}} - f_{\text{crystal}}} \tag{13}$$

with

$$f_{\text{cp}} = \frac{dW_{100-75}}{\rho_{\text{H2O}}\left(V/W_{\text{dry}}\right)_{\text{hcp}}} \tag{14}$$

where ρ_{H2O} is the density of water at 20 °C (0.9982 g/cm^3) and V and W_{dry} are the initial volume and 105 °C-dried mass of block sample. The masses of water in the capillary pores, or dW_{100-75}, are listed in エラー! 参照元が見つかりません。 to エラー! 参照元が見つかりません。 with the standard deviation in the supplementary data.

Fig. 15 shows the bulk creep modulus C_{gel}^{K} of C-S-H gel as a function of relative humidity. The bulk creep modulus C_{gel}^{K} increased almost linearly with decreasing drying relative humidity. For cement pastes with the same w/c ratio, the creep modulus of both the L-hcp and H-hcp at 100% relative humidity were equal. Similarly, at 11% relative humidity, the creep modulus of both L-hcp and H-hcp were equal. This suggests that for samples kept under a saturated condition, the creep modulus of the C-S-H gel depends on the w/c ratio but not on cement type, as well as at 11% drying relative humidity.

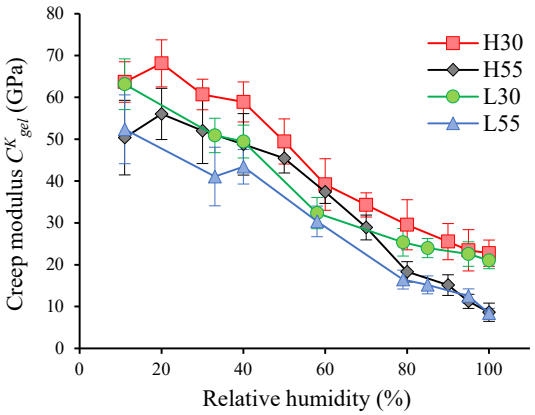

Fig. 15. Bulk creep modulus of C-S-H gel as a function of relative humidity after downscaling.

4.2 Colloidal features of the C-S-H gel

This section discusses the colloidal microstructure of C-S-H gel [19, 52] based on the water vapor sorption results presented in Section 3.2.

C-S-H gel consists of C-S-H sheets and interlayer space, which contains water [53] (see Fig. 18). Maruyama et al. [23, 26] suggested that the microstructure of C-S-H sheets and space between C-S-H sheets (i.e., basal space) can change when water is removed from the interlayer space upon drying, even though the degree of hydration remains unchanged. This change in microstructure is different when the paste is dried at relative humidity above 40% and below 40%.

When the paste is dried at a relative humidity above 40%, water first evaporates from the cement paste macropores followed by the mesopores, during which disjoining pressure induces a reduction of basal spacing in

467 the C-S-H gel, or the agglomeration of the C-S-H meso-structure [23, 54] . The sorption data presented in Fig. 7
468 shows that the sorption capacity is decreased from the saturated condition to 40%~50% drying relative humidity,
469 implying the reduction of basal spacing.
470 When dried at a relative humidity below 40%, the basal spacing remains stable. Some spaces around the C-
471 S-H agglomerations are segmented and have a high potential to adsorb water, so the sorption capacity can be
472 regained [26]. This is consistent with the increase of sorption capacity for drying relative humidity between 40%
473 and 11%, as shown in Fig. 7. It is suggested that the recovery of sorption capacity can be attributed to some
474 monolayers becoming the outer surface of blocks of C–S–H agglomerations due to the segmentation [26]. In effect,
475 the surface area remains constant when drying at a relative humidity between 40% to 11%, as shown in Fig. 9,
476 whereas sorption capacity increases.
477 As for BET surface area, Fig. 9 demonstrates the decrease in BET surface area with decreasing drying relative
478 humidity. However, Rahoui [55] observed, by comparing hcp samples dried at 11% relative humidity for six
479 months and re-humidified to 95% relative humidity, that the surface area of dried hcp recovered to its wet surface
480 area after re-humidification. This implies that the number of C-S-H sheets and their original surface area is kept
481 constant during drying. The apparent decrease of surface area as shown in Fig. 9 is only due to the change of basal
482 spacing, which is probably due to the decrease of the surface potential of the C-S-H sheets during segmentation or
483 slow water molecule migration into narrower interlayer spaces of the C-S-H sheets. Therefore, it is assumed that
484 the specific surface area at saturated condition can be taken as the referential surface area.
485
486 4.3 Discussion of the creep mechanism
487 This section discusses the creep mechanism based on the downscaled creep modulus and colloidal model of
488 C-S-H. Assuming that creep is due to sliding of C-S-H layers, the creep mechanism will be discussed using two
489 models from literature: the local microscopic relaxations model [36] and an atomistic simulation [37].
490 4.3.1 Apparent decrease of specific surface area and the microscopic relaxations model
491 In this section, the decrease of specific surface area as measured by water vapor sorption is discussed as a
492 cause for the change in creep modulus. This discussion is supported by the local microscopic relaxation model

493 [36], which considers the logarithmic creep behavior of cementitious materials a result of microscopic relaxation
494 of prestressed sites.

495 As explained in Section 4.2, the specific surface area at the saturated condition is considered as a referential
496 surface area corresponding to C-S-H for each type of cement paste. The difference in surface area between the
497 saturated condition and each drying state is defined as the reduction of surface area (ΔS_{H2O}) due to drying. The
498 relationship between the bulk creep modulus of C-S-H gel and ΔS_{H2O} is shown in Fig. 16. The bulk creep modulus
499 of the C-S-H gel correlates linearly well with ΔS_{H2O} for each cement paste. The negative values of ΔS_{H2O} were
500 presented as the surface area of the sample at saturated condition is not the maximum value in the case of L55.
501 For all four cement pastes, the bulk creep modulus was higher for higher ΔS_{H2O}. With greater reduction of surface
502 area, there is less space where C-S-H sheets can slide. Thus, the creep modulus increases when the drying relative
503 humidity is decreased. Similar explanations can be found in the local microscopic relaxation model.

504 In the exhaustive model of local microscopic relaxations [36] , the creep modulus C is proportional to
505 $(\Omega/\Omega_m)(1/\bar{n}_0)$, where Ω_m/Ω is the volume fraction of relaxation sites, and $\bar{n}_0$ is the number of relaxation sites
506 whose energy is in between U_0 and $U_0 + dU_0$ (Eq. 2.7 of [36]). If we consider that each microscopic relaxation is
507 some type of microcrack that then heals, at lower relative humidity, the microcrack is less pronounced than at a
508 higher relative humidity, i.e., Ω_m/Ω is lower for lower relative humidity. Alternatively, when the relative humidity
509 decreases, the relaxation becomes more difficult. In effect, all energy barriers at the relaxation site will be
510 increased, which results in a decrease in $\bar{n}_0$. This decrease in $\bar{n}_0$ approximately corresponds to the apparent
511 decrease of the specific surface area as shown Fig. 16.
512
513
514

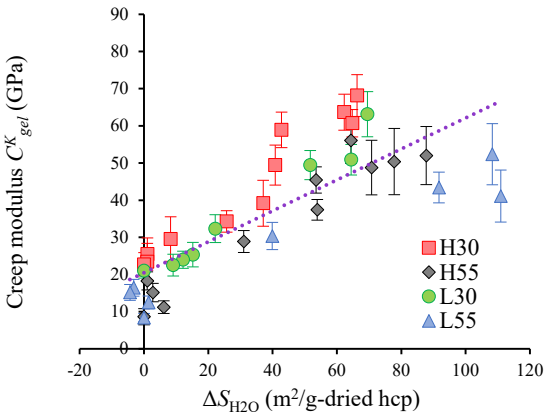

Fig. 16. The relationship between the bulk creep modulus of the C-S-H gel and the reduction of the water vapor surface area.

4.3.2 Statistically determined adsorption thickness as compared with results from atomistic simulation

The influence of water on sliding mechanics is discussed in this section. The variation of the creep modulus with respect to water will be compared with results from an atomistic simulation [37].

As explained in Section 4.2, taking the specific surface area at the saturated condition as a referential surface area corresponding to C-S-H for each type of cement paste, the adsorption thickness [56] was calculated as

$$t = \frac{w_{\text{evp}}/\rho_{\text{H2O,20°C}}}{S_{\text{H2O,sat}}} \quad (15)$$

where w_{evp} is the evaporable water content (g/g-dried hcp) from Fig. 4, $S_{\text{H2O,sat}}$ is the referential surface area at the saturated condition from the water vapor sorption isotherm (m^2/g-dried hcp), and $\rho_{\text{H2O,20°C}}$ is the density of water at 20 °C (998.2 kg/m^3).

In Fig. 17, the creep modulus of the drying C-S-H gel is plotted against the statistically determined thickness of the water. It appears that there is a threshold for the change of the C-S-H creep behavior. Above a water thickness of 1 nm, the creep modulus of the C-S-H gel does not change significantly when adsorption thickness decreases. Taking the cross sectional area of one water molecule as equal to 0.114 nm^2 [43], the thickness of one layer of water molecule is 0.263 nm at 20 °C. Hence, a thickness of 1 nm corresponds to approximately four water

molecule layers. In this high water content environment, the sliding of C-S-H sheets is easy and is not significantly affected by a change in water content. Below a thickness of 1 nm, a linear relationship between the bulk creep modulus and the statistical thickness of the water can be observed. For reduced water thickness, the sliding of C-S-H layers becomes more difficult, resulting in an increase of the creep modulus. Fig. 18 shows the schematic of the creep behavior of the C-S-H gel for different surrounding water states as determined by the water's statistical thickness. This concept with threshold at 1 nm of adsorption thickness is consistent with sliding free energy barrier calculations by Masoumi et al. [57]. Masoumi showed that the sliding free energy barrier for Tobermorite-like layers decreases exponentially as a function of layers separation distance and at roughly 0.8 nm the free energy is zero. In our results, the threshold value of statistical thickness of adsorption of 1 nm corresponds to 2 nm of layers separation, higher than the calculated value 0.8 nm of Masoumi et al. This may be explained by the following two points: firstly, the Tobermorite-like layers simulated by Masoumi et al. are straight, whereas in tested cement paste the layers of C-S-H are more likely to be winding hence sliding requires more energy; secondly, in amorphous C-S-H of cement paste more calcium ions are present in between silicate layers comparing to Tobermorite-like structure simulated by Masoumi et al, resulting in an increase of threshold value of layer separation distance which corresponds to zero free energy for sliding. A similar relationship between water and the creep modulus is also found by the atomistic simulation of [37], which proposed a correlation between the creep modulus of C-S-H gel and the molar ratio H/S of water to silica.

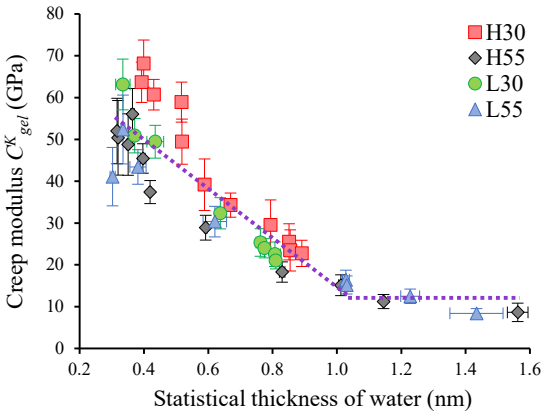

Fig. 17. The relationship between the bulk creep modulus of C-S-H gel and the statistical thickness of water.

In [37], the authors simulated the strain response of a C-S-H box under cyclic shear stress for different water contents. For each box, three stages were simulated: loading, unloading, and reloading. Supposing that creep is a phenomena in which the energy of a system gradually trends toward a lower minimum energy and given that a cyclic shear load can take a system to a more favorable local minimum in the energy landscape, they approximated the time-dependent creep strain behavior by cycle-dependent shear strain behavior. The strain in the reloading phase was fit by a logarithmic function, by which the same creep modulus as per Eq. (7) is obtained. In the following, this creep modulus is compared with the contact creep modulus from the indentation results.

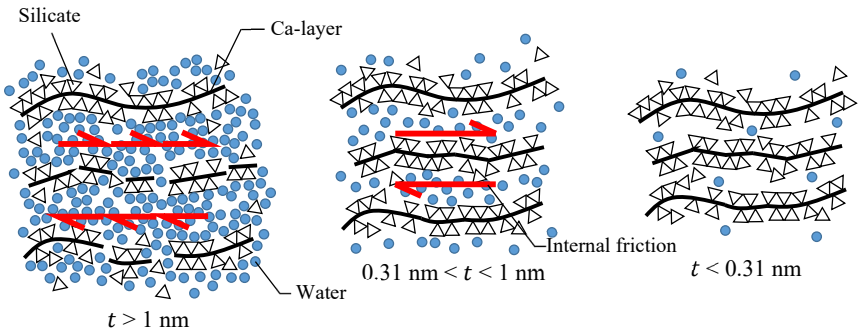

Fig. 18. Schematic of the creep behavior of C-S-H gel for different surrounding water states.

For the cement pastes that were used in the indentation test, the total molar ratio $(H/S)_{\text{total}}$ of water to silica was estimated by combining the Rietveld analysis of XRD results in Section 3.1 and the evaporable water content described in Section 3.2. The water content in the sample was considered as the sum of the chemically bounded water in C-S-H and the evaporable water. The mole number of the chemically bounded water was computed from the XRD results assuming that the molar ratio H/S of water to silica in C-S-H is equal to 2.5 [58] at 11% relative humidity. Then, all phases were transformed to the 105 °C state to normalize the chemically bounded water in C-S-H and evaporable water in the same state as described in [41]. Adding this chemically bounded water to the mole number of evaporable water, we obtain

$$\left(\frac{H}{S}\right)_{\text{total}} = \left(\frac{H}{S}\right)_{\text{CSH,105°C}} + \frac{W_{\text{evp}} m_{\text{total,105°C}}}{M_{\text{w}} S} \quad (16)$$

where $(H/S)_{\text{CSH,105°C}}$ is the molar ratio of water to silica per mass of C-S-H at 105 °C, obtained from XRD/Rietveld analysis based on an iterative process, S is the molar number of silica in C-S-H per volume of cement paste at 105 °C (mol), $m_{\text{total,105°C}}$ is the mass of cement paste per volume at 105 °C (g-dried hcp) from the XRD/Rietveld analysis, and M_{W} is the molecular weight of water, equal to 18.015 g/mol.

To investigate variation of the creep modulus with the variation of molar ratio $(H/S)_{\text{total}}$, the bulk creep modulus of C-S-H gel was normalized by the bulk creep modulus of C-S-H gel at $(H/S)_{\text{total}}$ = 4.5 for each type of cement paste. This normalized creep modulus $C^K_{gel}/C^K_{gel\ \text{at}\ H/S=4.5}$ is compared with the results of the atomistic simulation of [37] in Fig. 19. The change of creep modulus obtained from indentation results is consistent with those computed from atomistic simulation. Both results show the same trend of increasing creep modulus with decreasing molar ratio $(H/S)_{\text{total}}$. We therefore consider that our findings are consistent with the results of the atomistic simulation of [37].

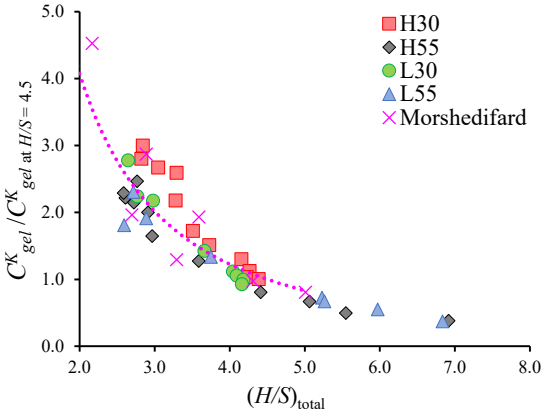

Fig. 19 The relationship between $C^K_{gel}/C^K_{gel\ \text{at}\ H/S=4.5}$ ratio and $(H/S)_{\text{total}}$.

5. Conclusion

Two types of hardened cement paste samples were examined under different relative humidities by using the microindentation technique. Their creep results were downscaled and the creep mechanism of C-S-H gel under different relative humidities was discussed. Several conclusions can be drawn:

- The bulk creep modulus of C-S-H gel increases when the drying relative humidity decreases.
- The creep mechanism of C-S-H can be explained by the sliding of C-S-H layers.
- Considering the surface area as sites where C-S-H layers can slide, a lower BET water vapor surface area results in a higher bulk creep modulus of the C-S-H gel.
- Considering adsorbed water on the surface of C-S-H layer to act as a lubricant for sliding of C-S-H layers, the creep modulus remains almost constant when the statistical thickness of the adsorbed water is higher than 1 nm. For statistical thicknesses of adsorption lower than 1 nm, the creep modulus increases with a decrease of adsorption thickness.
- Variation of the creep modulus of C-S-H with respect to drying relative humidity, obtained by the microindentation test, was found to be consistent with the local microscopic relaxation model.
- Correlation between the bulk creep modulus of C-S-H gel and the molar ratio of water to silica shows similar trends with those obtained from an atomistic simulation.

Acknowledgements

These experiments were financial sponsored by Japan Society for the Promotion of Science KAKENHI Grant Number 18H03804. The authors thank Dr. Matthieu Vandamme (École des Ponts ParisTech, Université Paris-Est, France) for his fruitful discussions and help in analyzing the results with the local microscopic relaxation model. The first author would like to gratefully acknowledge the scholarship of the Royal Thai Government.

References

[1] A. Bentur, R.L. Berger, F.V. Lawrence, N.B. Milestone, S. Mindess, J.F. Young, Creep and drying shrinkage of calcium silicate pastes III. A hypothesis of irreversible strains, Cem. Concr. Res., 9 (1979) 83-95.
[2] N.H. Brown, B.B. Hope, The creep of hydrated cement paste, Cem. Concr. Res., 6 (1976) 475-485.
[3] R.F. Feldman, Mechanism of creep of hydrated portland cement paste, Cem. Concr. Res., 2 (1972) 521-540.

[4] B.B. Hope, N.H. Brown, A model for the creep of concrete, Cem. Concr. Res., 5 (1975) 577-586.
[5] M. Vandamme, F.-J. Ulm, Nanogranular origin of concrete creep, Proc. Natl. Acad. Sci., 106 (2009) 10552.
[6] P.B. Zdenek, L. Guang-Hua, Comprehensive Database on Concrete Creep and Shrinkage, ACI Mater. J., 105.
[7] J. Němeček, Creep effects in nanoindentation of hydrated phases of cement pastes, Mater. Charact., 60 (2009) 1028-1034.
[8] C. Pichler, R. Lackner, Identification of Logarithmic-Type Creep of Calcium-Silicate-Hydrates by Means of Nanoindentation, Strain, 45 (2009) 17-25.
[9] J. Frech-Baronet, L. Sorelli, J.P. Charron, New evidences on the effect of the internal relative humidity on the creep and relaxation behaviour of a cement paste by micro-indentation techniques, Cem. Concr. Res., 91 (2017) 39-51.
[10] Y. Wei, S. Liang, X. Gao, Indentation creep of cementitious materials: Experimental investigation from nano to micro length scales, Constr. Build. Mater., 143 (2017) 222-233.
[11] Q. Zhang, R. Le Roy, M. Vandamme, B. Zuber, Long-term creep properties of cementitious materials: Comparing microindentation testing with macroscopic uniaxial compressive testing, Cem. Concr. Res., 58 (2014) 89-98.
[12] R. Le Roy, Déformations instantanées et différées des bétons à hautes performances, Ph.D. thesis, Ecole Nationale des Ponts et Chaussées, 1995.
[13] M. Vandamme, F.J. Ulm, Nanoindentation investigation of creep properties of calcium silicate hydrates, Cem. Concr. Res., 52 (2013) 38-52.
[14] D.-T. Nguyen, R. Alizadeh, J.J. Beaudoin, P. Pourbeik, L. Raki, Microindentation creep of monophasic calcium–silicate–hydrates, Cem. Concr. Compos., 48 (2014) 118-126.
[15] D.-T. Nguyen, R. Alizadeh, J.J. Beaudoin, L. Raki, Microindentation creep of secondary hydrated cement phases and C–S–H, Mater. Struct., 46 (2013) 1519-1525.
[16] B.T. Tamtsia, J.J. Beaudoin, J. Marchand, Time-dependent load-induced deformation of Ca(OH)2, Adv. Cem. Res., 14 (2002) 135-139.
[17] G. Constantinides, F.-J. Ulm, The effect of two types of C-S-H on the elasticity of cement-based materials: Results from nanoindentation and micromechanical modeling, Cem. Concr. Res., 34 (2004) 67-80.
[18] A. Aili, M. Vandamme, J.-M. Torrenti, B. Masson, Is long-term autogenous shrinkage a creep phenomenon induced by capillary effects due to self-desiccation?, Cem. Concr. Res., 108 (2018) 186-200.
[19] H.M. Jennings, Refinements to colloid model of C-S-H in cement: CM-II, Cem. Concr. Res., 38 (2008) 275-289.
[20] E. Masoero, E. Del Gado, R.J.M. Pellenq, S. Yip, F.-J. Ulm, Nano-scale mechanics of colloidal C–S–H gels, Soft Matter, 10 (2014) 491-499.
[21] G.W. Scherer, Structure and properties of gels, Cem. Concr. Res., 29 (1999) 1149-1157.
[22] J.J. Thomas, H.M. Jennings, A colloidal interpretation of chemical aging of the C-S-H gel and its effects on the properties of cement paste, Cem. Concr. Res., 36 (2006) 30-38.
[23] I. Maruyama, G. Igarashi, Y. Nishioka, Bimodal behavior of C-S-H interpreted from short-term length change and water vapor sorption isotherms of hardened cement paste, Cem. Concr. Res., 73 (2015) 158-168.
[24] I. Maruyama, Y. Nishioka, G. Igarashi, K. Matsui, Microstructural and bulk property changes in hardened cement paste during the first drying process, Cem. Concr. Res., 58 (2014) 20-34.
[25] I. Maruyama, T. Ohkubo, T. Haji, R. Kurihara, Dynamic microstructural evolution of hardened cement paste during first drying monitored by 1H NMR relaxometry, Cem. Concr. Res., 122 (2019) 107-117.
[26] I. Maruyama, N. Sakamoto, K. Matsui, G. Igarashi, Microstructural changes in white Portland cement paste under the first drying process evaluated by WAXS, SAXS, and USAXS, Cem. Concr. Res., 91 (2017) 24-32.
[27] Z.P. Bazant, J.C. Chern, Concrete creep at variable humidity: constitutive law and mechanism, Mater. Struct., 18 (1985) 1.
[28] D.J. Hannant, The mechanism of creep in concrete, Matériaux et Construction, 1 (1968) 403-410.
[29] S. Mallick, M.B. Anoop, K. Balaji Rao, Early age creep of cement paste - Governing mechanisms and role of water-A microindentation study, Cem. Concr. Res., 116 (2019) 284-298.
[30] E.A. Pachon-Rodriguez, E. Guillon, G. Houvenaghel, J. Colombani, Wet creep of hardened hydraulic cements — Example of gypsum plaster and implication for hydrated Portland cement, Cem. Concr. Res., 63 (2014) 67-74.
[31] I. Pignatelli, A. Kumar, R. Alizadeh, Y. Le Pape, M. Bauchy, G. Sant, A dissolution-precipitation mechanism is at the origin of concrete creep in moist environments, J. Chem. Phys., 145 (2016) 054701.
[32] B.T. Tamtsia, J.J. Beaudoin, Basic creep of hardened cement paste A re-examination of the role of water, Cem. Concr. Res., 30 (2000) 1465-1475.
[33] P. Bažant Zdeněk, B. Hauggaard Anders, S. Baweja, F.-J. Ulm, Microprestress-Solidification Theory for Concrete Creep. I: Aging and Drying Effects, J. Eng. Mech., 123 (1997) 1188-1194.

[34] A.B. Giorla, C.F. Dunant, Microstructural effects in the simulation of creep of concrete, Cem. Concr. Res., 105 (2018) 44-53.
[35] P. Rossi, J.-L. Tailhan, F. Le Maou, L. Gaillet, E. Martin, Basic creep behavior of concretes investigation of the physical mechanisms by using acoustic emission, Cem. Concr. Res., 42 (2012) 61-73.
[36] M. Vandamme, Two models based on local microscopic relaxations to explain long-term basic creep of concrete, Proc. R. Soc. A, Math. Phys. Eng. Sci., 474 (2018) 20180477.
[37] A. Morshedifard, S. Masoumi, M.J. Abdolhosseini Qomi, Nanoscale origins of creep in calcium silicate hydrates, Nat. Commun., 9 (2018) 1785.
[38] J. Bisschop, F.K. Wittel, Contraction gradient induced microcracking in hardened cement paste, Cem. Concr. Compos., 33 (2011) 466-473.
[39] L. Greenspan, Humidity fixed points of binary saturated aqueous solutions, J. Res. Natl. Bur. Stand., Phys. Chem., 81A (1977) 89-96.
[40] R.H. Stokes, R.A. Robinson, Standard Solutions for Humidity Control at 25° C, Ind. Eng. Chem., 41 (1949) 2013-2013.
[41] I. Maruyama, G. Igarashi, Cement Reaction and Resultant Physical Properties of Cement Paste, J. Adv. Concr. Technol., 12 (2014) 200-213.
[42] S. Brunauer, P.H. Emmett, E. Teller, Adsorption of Gases in Multimolecular Layers, J. Am. Chem. Soc., 60 (1938) 309-319.
[43] I. Odler, The BET-specific surface area of hydrated Portland cement and related materials, Cem. Concr. Res., 33 (2003) 2049-2056.
[44] L.Y. Gómez-Zamorano, J.I. Escalante-García, Effect of curing temperature on the nonevaporable water in portland cement blended with geothermal silica waste, Cem. Concr. Compos., 32 (2010) 603-610.
[45] M. Mouret, A. Bascoul, G. Escadeillas, Study of the degree of hydration of concrete by means of image analysis and chemically bound water, Advanced Cement Based Materials, 6 (1997) 109-115.
[46] Q. Zhang, Creep properties of cementitious materials : effect of water and microstructure : An approach by microindentation, Ph.D. thesis, Université Paris-Est, 2014.
[47] I. Baauerizo, T. Matschei, K. Scrivener, Impact of water activity on the water content of cement hydrates, 2012, pp. 249-260.
[48] I. Maruyama, E. Gartner, K. Beppu, R. Kurihara, Role of alcohol-ethylene oxide polymers on the reduction of shrinkage of cement paste, Cem. Concr. Res., 111 (2018) 157-168.
[49] I. Maruyama, J. Rymeš, M. Vandamme, B. Coasne, Cavitation of water in hardened cement paste under short-term desorption measurements, Mater. Struct., 51 (2018) 159.
[50] O. Bernard, F.-J. Ulm, J.T. Germaine, Volume and deviator creep of calcium-leached cement-based materials, Cem. Concr. Res., 33 (2003) 1127-1136.
[51] A. Aili, M. Vandamme, J.-M. Torrenti, B. Masson, J. Sanahuja, Time evolutions of non-aging viscoelastic Poisson's ratio of concrete and implications for creep of C-S-H, Cem. Concr. Res., 90 (2016) 144-161.
[52] H.M. Jennings, A model for the microstructure of calcium silicate hydrate in cement paste, Cem. Concr. Res., 30 (2000) 101-116.
[53] R.F. Feldman, P.J. Sereda, A model for hydrated Portland cement paste as deduced from sorption-length change and mechanical properties, Matériaux et Construction, 1 (1968) 509-520.
[54] W.A. Gutteridge, L.J. Parrott, A study of the changes in weight, length and interplanar spacing induced by drying and rewetting synthetic CSH (I), Cem. Concr. Res., 6 (1976) 357-366.
[55] H. Rahoui, Contribution to understanding the action of shrinkage reducing admixtures in cementitious materials: experiments and modelling, Ph.D. thesis, Université Paris-Est, 2018.
[56] R. Badmann, N. Stockhausen, M.J. Setzer, The statistical thickness and the chemical potential of adsorbed water films, J. Colloid Interface Sci., 82 (1981) 534-542.
[57] S. Masoumi, H. Valipour, M.J. Abdolhosseini Qomi, Interparticle Interactions in Colloidal Systems: Toward a Comprehensive Mesoscale Model, ACS Applied Materials & Interfaces, 9 (2017) 27338-27349.
[58] R.F. Feldman, V.S. Ramachandran, Microstructure of calcium hydroxide depleted portland cement paste I: Density and helium flow measurements, Cem. Concr. Res., 12 (1982) 179-189.

#